

Design Optimization Model for an Automotive Electric Water Pump

James T. Allison
optimize@umich.edu
Optimal Design Laboratory
The University of Michigan

Revised: September 3, 2007

1 Introduction

This report describes a design optimization model for an automotive water (coolant) pump driven by a DC electric motor. It is intended for use as an example problem for multidisciplinary design optimization (MDO) methods, and consists of several interacting analysis functions. These analysis functions are based on sets explicit algebraic equations, making this model easily reproduced for use in MDO studies. A similar model was presented in [1] that involved the design of a belt-driven electric sump pump. The model presented here is more sophisticated, and uses an alternative approach to solve for the steady state operating speed. In [1] the analysis functions generated torque-speed curves for the pump and motor, and then solved for the intersection of those curves to find the operating point. Generating these curves was costly, but eliminated some of the feedback coupling between analysis functions. In this model the operating speed is treated as a coupling variable [2], and instead of determining the operating speed via torque-speed curves, it is solved for as an unknown state variable. This results in strong coupling between analysis functions, but makes for a more interesting analysis structure for analysis of MDO methods.

Traditional automotive water pumps are belt driven by the vehicle engine, constraining pump shaft speed to engine speed multiplied by the belt speed ratio. In some cases, such as idling after a period of high load, the water pump must provide flow and pressure sufficient to cool a hot engine at low shaft speeds. Pumps can be designed to operate efficiently at a specific operating point, but cannot be simultaneously efficient at high and low shaft speeds. An engine-driven pump operates at off-design flow conditions during much of its duty cycle due to large speed fluctuations, requiring more input power than a pump driven by a constant-speed source. A motor-driven pump can

provide constant input speed, and also consumes less energy by only pumping when when needed. Traditional water pumps are run continuously and utilize a thermostat-controlled bypass when engine cooling is not required.

Electrification of belt-driven automotive components is a promising means for improving fuel economy. Electrification of some components, such as cooling fans, has been incorporated for some time into production vehicles. Electrification of additional components is a more recent endeavor [3, 4, 5]. Surampudi et al. tested a speed-controlled electric water pump on a class-8 tractor and measured an 80% reduction in energy consumption [6].

The analysis model used in this design problem involves five interdependent analysis functions that compute performance metrics based on ten design variable values. These quantities are defined in Table 1. Design variables x_1 – x_5 define motor geometry, and x_6 – x_{10} define pump geometry. The motor is a permanent magnet brushed DC electric motor with four pole pairs, and the pump is single-stage centrifugal with six impeller blades and a single diffuser vane (Fig. 1). The motor directly drives the pump, so their shaft speeds are identical: $\omega_{\text{motor}} = \omega_{\text{pump}} = \omega$.

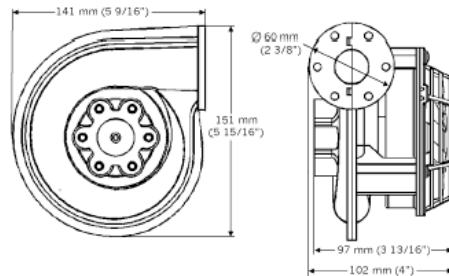


Figure 1: Electrically driven centrifugal water pump

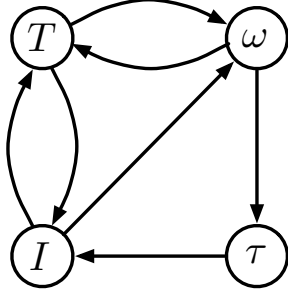


Figure 2: Analysis interactions in electric water pump model

Several analysis interactions are modeled. For example, the temperature is computed based on the motor current and speed, but the temperature affects the electrical resistance and current, and the current influences the motor speed. The interdependence between analysis functions is illustrated in Fig. 2. The details of these interactions are described in subsequent sections. Since pump pressure P and input shaft torque τ depend on identical sets of design variables and analysis outputs, only τ is included in the graph for simplicity and represents both P and τ calculations.

All model interactions and design variable dependence can be compactly represented using an adjacency matrix [7]. This matrix corresponds to a directed graph whose vertices are the design variables and analysis

functions for the model of an engineering system. Arcs in the graph indicate the existence of a dependence relationship. Half of the matrix rows can be omitted without loss of information since design variables are independent quantities and are therefore source vertices in the directed graph. The adjacency matrix for the water pump model is:

$$\mathbf{A} = \begin{array}{c|cccccccccccc} & T & I & \omega & \tau & d & d_2 & d_3 & L & \ell_c & D_2 & b & \beta_1 & \beta_2 & \beta_3 \\ \hline T & 0 & 1 & 1 & 0 & 1 & 1 & 1 & 1 & 1 & 0 & 0 & 0 & 0 & 0 \\ I & 1 & 0 & 0 & 1 & 1 & 1 & 1 & 1 & 0 & 0 & 0 & 0 & 0 & 0 \\ \omega & 1 & 1 & 0 & 0 & 1 & 1 & 1 & 1 & 1 & 0 & 0 & 0 & 0 & 0 \\ \tau & 0 & 0 & 1 & 0 & 0 & 0 & 0 & 0 & 0 & 1 & 1 & 1 & 1 & 1 \end{array}$$

The design problem, formally stated in Problem (1) is to minimize the electric power P_e consumed by the water pump, while ensuring sufficient pressure differential, safe motor temperature, compatible axial motor length, and a desired flow rate.

$$\begin{aligned} \min_{\mathbf{x}} \quad & P_e = VI \\ \text{subject to} \quad & P \geq P_{min} = 100 \text{ kPa} \\ & T \leq T_{max} = 428 \text{ K} \\ & L + \ell_c \leq 0.2 \text{ m} \\ & Q = 1.55 \cdot 10^{-3} \text{ m}^3/\text{sec} \end{aligned} \tag{1}$$

The source voltage V is 14.4 volts. The pressure differential and flow constraints ensure the engine is adequately cooled. The flow constraint is implicitly satisfied during the torque and pressure analysis. The temperature constraint ensures the motor wire insulation is not damaged, and the constraint on motor axial length ($L + \ell_c$) is required for packaging.

The analysis functions are very strongly coupled; first and second-order algorithms failed in most cases to find a solution to the system of equations in Table 1. The design problem was successfully solved using mesh adaptive direct search [8] and the individual disciplinary feasible (IDF) formulation [9]. The minimal power consumption is 140 W, a substantial improvement over traditional water pumps of similar capacity, which consume nearly 300 W continuously [4]. The following sections describe in detail the calculation of each of the five analysis functions.

2 Analysis Overview

The functions in Table 1 are evaluated by solving systems of nonlinear algebraic equations that approximate motor and pump behavior under steady state operating conditions. Several equations are coupled and require iterative solution techniques. The motor winding

Table 1: Analysis functions and design variables for the electric water pump design problem

| Analysis Functions | |
|---|-----------------------------|
| $T = a_1(I, \omega, d, d_2, d_3, L, \ell_c)$ | Mot. winding temp. (K) |
| $I = a_2(\tau, T, d, d_2, d_3, L)$ | Motor current (amps) |
| $\omega = a_3(I, T, d, d_2, d_3, L, \ell_c)$ | Motor speed (rad/sec) |
| $\tau = a_4(\omega, D_2, b, \beta_1, \beta_2, \beta_3)$ | Pump drive torque (Nm) |
| $P = a_5(\omega, D_2, b, \beta_1, \beta_2, \beta_3)$ | Pressure differential (kPa) |

| Design Variables | |
|--------------------|-----------------------------------|
| $x_1 = d$ | Motor wire diameter (m) |
| $x_2 = d_2$ | Inner motor armature diameter (m) |
| $x_3 = d_3$ | Outer motor armature diameter (m) |
| $x_4 = L$ | Motor armature length (m) |
| $x_5 = \ell_c$ | Motor commutator length (m) |
| $x_6 = D_2$ | Pump impeller diameter (m) |
| $x_7 = b$ | Pump impeller blade width (m) |
| $x_8 = \beta_1$ | Pump blade angle at inlet (rad) |
| $x_9 = \beta_2$ | Pump blade angle at outlet (rad) |
| $x_{10} = \beta_3$ | Pump diffuser inlet angle (rad) |

temperature T is computed using a thermal resistance model similar to that found in [10], adapted for permanent magnet DC motors. Additional heat transfer correlations were obtained from [11]. The motor current I and shaft speed ω are computed based on fundamental DC motor equations [12, 13] adapted to the specific geometry of this motor. The pump drive torque and pressure differential are computed for a prescribed flow rate Q using fluid mechanics equations for centrifugal pumps [14]. Model parameters used in this analysis are listed in Table 2. Motor and pump geometry will be described, followed by description of the analysis equations. Full description of the physics underlying the equations presented is omitted for brevity, and the reader is referred to the references for more details.

Table 2: Model parameters

| | | |
|------------|-------------------|--|
| δ_a | 0.002 | motor air gap (m) |
| δ_h | 0.010 | motor housing thickness (m) |
| d_1 | 0.008 | motor shaft diameter (m) |
| g | 9.81 | gravitational constant (m/s^2) |
| T_∞ | 350 | engine compartment temp. (K) |
| n_a | 1.50 | slot/tooth ratio |
| p | 4 | one-half number of poles |
| n_p | 0.55133 | wire packing ratio |
| μ_0 | 18.27e-6 | viscosity constant (Pa·s) |
| T_0 | 291.15 | base temperature (K) |
| C | 120 | viscosity parameter (K) |
| C_p | 1.009 | air heat capacity (kJ/kg·K) |
| B_r | 0.10 | remnant magnetic flux density (T) |
| V | 14.4 | source voltage (V) |
| D_s | 0 | pump shaft diameter (m) |
| D_1 | 0.020 | impeller inlet diameter (m) |
| D_3 | 0.150 | volute throat mean inlet diameter (m) |
| D_4 | 0.032 | exit flange inner diameter (m) |
| n_B | 6 | no. impeller blades |
| n_V | 1 | no. diffuser vanes |
| b_3 | 0.032 | diffuser inlet width (m) |
| ρ_c | 970 | coolant density (kg/m^3) |
| Q | 0.00155 | flow rate (m^3/s) |
| C_{DF} | $1 \cdot 10^{-7}$ | disk friction coefficient ($\text{m}^2\text{s}^2/\text{kg}$) |
| C_{SF} | $5 \cdot 10^{-3}$ | skin friction coefficient (m^{-1}) |
| C_{VD} | 0.5 | diffuser loss coefficient |
| C_{in} | 0.8 | diffuser approach coefficient |

2.1 Motor Geometry

Figure 3 provides a side section view of the DC motor. The iron-cored armature, or rotor, of the DC motor rotates within cylindrical permanent magnets with

remnant magnetic flux density B_r . The outer armature diameter is d_3 , the armature axial length is L , and the gap between the armature and magnets is δ_a . The thickness of the magnets is δ_h . A shaft of diameter d_1 runs through the armature and is supported by bearings at each end of the motor housing. The commutator is a mechanical switch that routes electrical current through the correct armature windings at the appropriate time as the motor rotates. Stationary brushes sliding on the commutator provide the means for electrical conduction (brushes not shown). The commutator is mounted on the motor shaft and has outer diameter d_c and axial length ℓ_c .

Armature geometry is approximated as shown in Fig. 4. Insulated copper windings with diameter d run through each of the $2p = 8$ armature slots, where p is the number of magnetic pole pairs. Each slot has a depth of $(d_3 - d_2)/2$ and subtends the angle θ_s . The armature teeth separate the windings and each tooth subtends an angle of θ_t .

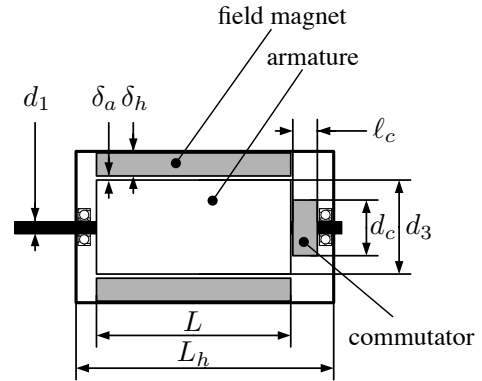


Figure 3: Schematic of permanent magnet DC motor

2.2 Pump Geometry

Figure 5 illustrates the geometry of the centrifugal water pump. The drive shaft of diameter D_s rotates the impeller, which has $n_B = 6$ blades. Coolant flows in through the inlet of diameter and is expelled radially outwards due to impeller rotation. As the coolant flows through the diffuser its velocity is reduced, but experiences an increase in pressure according to Bernoulli's principle. The outer impeller diameter is D_2 , and the volute inlet diameter is D_3 . The inlet impeller blade angle is β_1 , and the outlet impeller blade angle is β_2 . The diffuser inlet blade angle (not shown) is β_3 . The exit flange diameter is D_4 . The impeller blade width is b and the diffuser inlet width is b_3 .

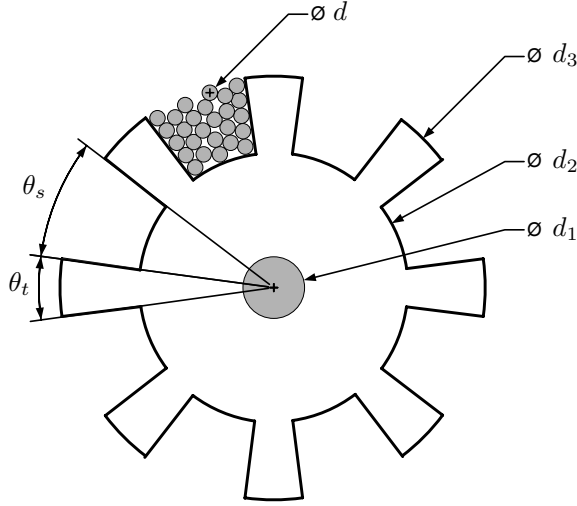


Figure 4: Section view of DC motor armature

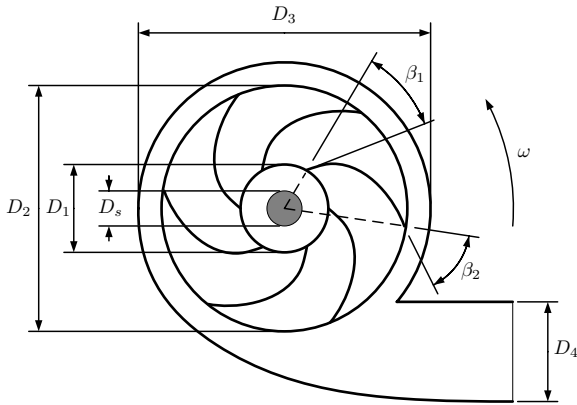


Figure 5: Schematic of centrifugal water pump

3 Thermal Analysis

The objective of the thermal analysis is to compute the armature winding temperature T given motor geometry and operating conditions. Motor geometry is simplified to enable analysis using a thermal resistance model. All heat generation is assumed to originate from armature windings, evenly distributed throughout the annular cylinder containing armature windings with outer diameter d_3 , inner diameter d_2 , and length L . First it will be shown how to compute heat generation due to I^2R losses. The thermal circuit and equations will then be presented, followed by a description of the solution process for the thermal analysis.

3.1 Wire Length and Heat Generation

Calculation of heat generation requires knowledge of armature electrical resistance, which depends on total wire length and wire temperature. The model for wire length assumes windings are made around each armature tooth, and accounts for wire curvature and extension beyond armature ends. The slot to tooth volume ratio, $n_a = \theta_s/\theta_t$, is assumed to be fixed at 1.5. The total volume occupied by wire passing through the slots V_s can be calculated using the following formulae:

$$\theta_s = \pi/p(1 + 1/n_a), \theta_t = \theta_s/n_a, \theta_p = \theta_s + \theta_t$$

$$A_s = \theta_s(d_3^2 - d_2^2)/8, V_s = n_p A_s L$$

where θ_p is the angle between poles, A_s is the section area of each slot, and $n_p = 0.55133$ is the packing ratio, i.e., the ratio of wire volume occupying slots to total slot volume. The ratio n_p was calculated based on close packing geometry. $A_w = \pi d^2/4$ is the sectional area of a single wire, and the total length of wire passing through armature slots is $\ell_s = V_s/A_w$. The total number of winding turns for all poles is $n_t = \ell_s/2L$. In reality n_t is integer valued, but is assumed to be relaxed to a continuous number here. This provides a reasonable approximation when n_t is large. The average wire length between slots for each winding turn is $\ell_e = \theta_s(1/n_a + \pi/4)(d_2 + d_3)/4$, and the total length of wire is:

$$\ell = \ell_s + 2\bar{\ell}_e n_t \quad (2)$$

The resistivity of copper varies with temperature, and is approximated using a linear model:

$$\rho(T) = 1.72 \cdot 10^{-8}(1 + 0.00393(T - 293)) \quad (3)$$

The total heat generated by the armature windings due to I^2R losses is:

$$S = 4\rho\ell I^2/\pi d^2 \quad (4)$$

3.2 Thermal Resistance Model

The thermal resistance model used in this analysis to calculate wire temperature T is illustrated in Fig. 6. The heat source is the annulus ring of the armature containing the windings, and the thermal sink is the engine compartment at temperature T_∞ .

The first path in the circuit passes through R_1 , R_2 , and R_3 , and represents the thermal path directly from the armature through the air gap, magnets, and housing to the engine compartment. All other thermal energy flows inward through the inner armature R_4 , and then through the shaft to either side of the motor. The

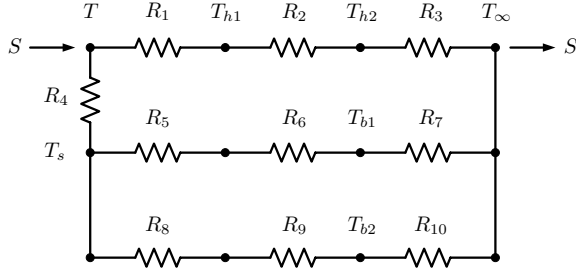


Figure 6: DC motor thermal resistance model

path through R_5 , R_6 , and R_7 corresponds to the side with the commutator, and the remaining path corresponds to the side without the commutator.

Before the thermal resistance formulae are detailed, models for material property dependence on temperature are presented. These are used in many of the resistance calculations. The models for air viscosity, density, and conductivity are:

$$\mu_{air}(T) = \mu_0(T_0 + C)(T/T_0)^{3/2}/(T + C) \quad (5)$$

$$\rho_{air}(T) = 1.01325/287.05T \quad (6)$$

$$k_{air}(T) = 1.5207 \cdot 10^{-11}T^3 - 4.8574 \cdot 10^{-8}T^2 + 1.0184 \cdot 10^{-4}T - 3.9333 \cdot 10^{-4} \quad (7)$$

The model for iron conductivity is linear:

$$k_{fe}(T) = 110.4676 - 0.1002T \quad (8)$$

R_1 : Convection between armature and field magnets

The Reynold's and Nusselt numbers for the gap between the armature and field magnets are $Re_1 = \omega d_3^2 \rho_{air}(T)/2\mu_{air}(T)$ and $Nu_1 = 0.318Re_1^{0.571}$, respectively. The convective thermal resistance between the the armature and field magnets is:

$$R_1 = 2/Nu_1 k_{air}(T) \quad (9)$$

R_2 : Conduction through field magnets and housing

The resistance due to the thin motor housing is considered negligible compared to that of the field magnets, so only one material is considered in this resistance calculation. The inner diameter of the field magnets is

$d_4 = d_3 + 2\delta_a$, and the outer diameter of the housing is $d_5 = d_4 + 2\delta_h$. The temperature of the inner magnet surface is T_{h1} and the temperature of the outer housing surface is T_{h2} . The thermal conductivity of the field magnets is calculated using Eq. (8) and the average magnet temperature $\bar{T}_h = (T_{h1} + T_{h2})/2$. The thermal resistance due to conduction through the field magnets and housing is:

$$R_2 = \ln(d_5/d_4)/(2\pi L k_{fe}(\bar{T}_h)) \quad (10)$$

R_3 : Convection from housing to engine compartment

The total length of the motor housing, accounting for space for bearings and clearance, is approximated as $L_h = L + 1.5\ell_c + 2d_1$. The volumetric thermal expansion coefficient in the calculation of R_3 is approximated as $\beta_{t3} = 1/T_{h2}$. The kinematic viscosity of air in this region is $\nu_{air3} = \mu_{air}(T_{h2})/\rho_{air}(T_{h2})$. The air heat capacity is $C_p = 1.009$, and the thermal diffusivity here is $\alpha_3 = k_{air}(T_{h2})/C_p \rho_{air}(T_{h2})$. The Prandtl number here is $Pr_3 = \nu_{air3}/\alpha_3$, and the Rayleigh and Nusselt numbers are:

$$Ra_3 = g\beta_{t3}(T_{h2} - T_\infty)L_h^3/\alpha_3\nu_{air3}$$

$$Nu_3 = \left(0.6 + \frac{0.387Ra_3^{1/6}}{((1 + (0.559/Pr_3)^{9/16})^{8/27})} \right)^2$$

The thermal resistance due to free convection from the motor housing to the engine compartment is:

$$R_3 = 2/(k_{air}(T_{h2})Nu_3L_h) \quad (11)$$

R_4 : Conduction through armature core

The conductivity of the core is based on the average between the winding and shaft temperatures: $T_c = (T + T_s)/2$. It is assumed that the shaft within the core is at a constant temperature T_s throughout its volume and has no thermal resistance. The thermal conductivity resistance through the armature core is:

$$R_4 = \ln(d_2/d_1)/2\pi L k_{fe}(T_c) \quad (12)$$

R_5 : Conduction through motor shaft and bearings on commutator side

The section area of the shaft is $A_s = \pi d_1^2/4$, and the length of the shaft extending beyond the armature is $L_s = 1.5\ell_c + d_1$. The thermal resistance through the support bearing is assumed to be a constant 1.5 K/W. The thermal resistance through this section of shaft is:

$$R_5 = L_s/A_s k_{fe}(T_s) + 1.5 \quad (13)$$

R_6 and R_9 : Conduction through motor end bells

The motor end bells are the disk-shaped portions of the housing at each end of the motor. It is assumed that the conductive resistance through both end bells is negligible. Therefore, $R_6 = R_9 = 0$.

 R_7 : Convection between end bell and engine compartment on commutator side

The volumetric thermal expansion coefficient in the calculation of R_7 is approximated as $\beta_{t7} = 1/T_{b1}$, where T_{b1} is the temperature of the commutator side end bell. The kinematic viscosity is $\nu_{air7} = \mu_{air}(T_{b1})/\rho_{air}(T_{b1})$, and the thermal diffusivity is $\alpha_7 = k_{air}(T_{b1})/C_p\rho_{air}(T_{b1})$. The Prandtl number is $Pr_7 = \nu_{air7}/\alpha_7$, and the Rayleigh and Nusselt numbers are:

$$Ra_7 = g\beta_{t7}(T_{b1} - T_\infty)d_3^3/\nu_{air7}\alpha_7$$

$$Nu_7 = \left(0.825 + \frac{(0.387Ra_7^{1/6})}{(1 + (0.492/Pr_7)^{9/16})^{8/27}}\right)^2$$

The thermal resistance due to free convection from the commutator side end bell to the engine compartment is:

$$R_7 = 8/\pi Nu_7 d_4 k_{air}(T_{b1}) \quad (14)$$

 R_8 : Conduction through motor shaft and bearings on non-commutator side

The thermal resistance through the section of motor shaft extending beyond the armature on the non-commutator side is:

$$R_8 = 4/\pi d_1 k_{fe}(T_s) + 1.5 \quad (15)$$

 R_{10} : Convection between end bell and engine compartment on non-commutator side

The volumetric thermal expansion coefficient in the calculation of R_{10} is approximated as $\beta_{t10} = 1/T_{b2}$, where T_{b2} is the temperature of the non-commutator side end bell. The kinematic viscosity is $\nu_{air10} = \mu_{air}(T_{b2})/\rho_{air}(T_{b2})$, and the thermal diffusivity is $\alpha_{10} = k_{air}(T_{b2})/C_p\rho_{air}(T_{b2})$. The Prandtl number is $Pr_{10} = \nu_{air10}/\alpha_{10}$, and the Rayleigh and Nusselt numbers are:

$$Ra_{10} = g\beta_{t10}(T_{b2} - T_\infty)d_3^3/\nu_{air10}\alpha_{10}$$

$$Nu_{10} = \left(0.825 + \frac{0.387Ra_{10}^{1/6}}{(1 + (0.492/Pr_{10})^{9/16})^{8/27}}\right)^2$$

The thermal resistance due to free convection from the non-commutator side end bell to the engine compartment is:

$$R_{10} = 8/\pi Nu_{10} d_4 k_{air}(T_{b2}) \quad (16)$$

Temperature equations

The total thermal resistance R and several intermediate resistance quantities are required for solution of the system temperatures:

$$R_{1,2,3} = R_1 + R_2 + R_3$$

$$R_{5,6,7} = R_5 + R_6 + R_7$$

$$R_{8,9,10} = R_8 + R_9 + R_{10}$$

$$R_{5-10} = 1/(1/R_{5,6,7} + 1/R_{8,9,10})$$

$$R_{4-10} = R_4 + R_{5-10}$$

$$R = 1/(1/R_{1,2,3} + 1/R_{4-10})$$

With these resistances defined we can now present the coupled system of equations based on the circuit in Fig. 6 that model the steady state thermal behavior of the DC motor:

$$T = T_\infty + RS \quad (17a)$$

$$\Delta T = T - T_\infty \quad (17b)$$

$$q_{p1} = \Delta T/R_{1,2,3} \quad (17c)$$

$$q_{p2} = \Delta T/R_{4-10} \quad (17d)$$

$$T_{h1} = T - q_{p1}R_1 \quad (17e)$$

$$T_{h2} = T_{h1} - q_{p1}R_2 \quad (17f)$$

$$T_s = T - q_{p2}R_4 \quad (17g)$$

$$q_{p3} = (T_s - T_\infty)/R_{5,6,7} \quad (17h)$$

$$q_{p4} = (T_s - T_\infty)/R_{8,9,10} \quad (17i)$$

$$T_{b1} = T_s - q_{p3}(R_5 + R_6) \quad (17j)$$

$$T_{b2} = T_s - q_{p4}(R_8 + R_9) \quad (17k)$$

where ΔT is the temperature drop between the armature windings and the engine compartment, and q_{p1} , q_{p2} , q_{p3} , and q_{p4} are heat flows through circuit paths formed by $R_{1,2,3}$, R_{4-10} , $R_{5,6,7}$, and $R_{8,9,10}$, respectively. Since many thermal resistance values depend on temperature values the system of equations is coupled, and must be solved using an iterative technique. A least squares approach has been found to be more successful at solving this system than nonlinear Gauss-Seidel or Newton's method.

4 Motor Current Analysis

The motor current model predicts the current through the motor armature I given the armature temperature T , required motor shaft torque τ , and motor geometry. The magnetic field depends on temperature and is approximated using the formula:

$$B = B_r(1 - 0.0017(T - 293))$$

where B_r is the remanent magnetic flux density (assumed constant). The magnetic flux is $\phi = \pi(d_2 + d_3)LB/2$, and the total number of conductors in the magnetic field is $Z = 2n_t$. The calculation for the number of winding turns n_t was given in Section 3.1. The motor current is:

$$I = \tau\pi/\phi pZ \quad (18)$$

5 Motor Speed Analysis

The objective of this analysis is to compute the motor speed ω given the motor current I and armature temperature T . The model accounts for both the electrical resistance through the armature windings and the voltage drop across the commutator. The resistance through the windings is $R_a = 4\rho\ell/\pi d^2$. Recall that Eq. (4) is used to model the dependence of copper resistivity on temperature. The length ℓ is computed according to the formulae in Section 3.1. The back emf, i.e., voltage generated due to motor rotation that opposes source voltage, is $\mathcal{E} = R_a I$. The voltage drop across the commutator consists of two components:

$$\Delta V_c = \Delta V_{c1} + \Delta V_{c2}$$

A model for each component was developed based on empirical data from [12]:

$$\Delta V_{c1} = 0.8692 - 0.6458 \cdot e^{-0.8207\rho_I}$$

$$\Delta V_{c2} = 1.0037 - 0.5912 \cdot e^{-1.32\rho_I}$$

where $\rho_I = I/A_b$ is the current density at the commutator/brush interface, and $A_b = \pi d_c \ell_c/2$ is the brush contact area. It is assumed here that the commutator diameter is proportional to armature diameter: $d_c = d_3/2$. The motor speed is:

$$\omega = 2\pi(V - \Delta V_c - IR_a)/\phi Z p \quad (19)$$

6 Torque and Pressure Analysis

The analysis presented in this section computes the torque τ required to drive the pump at the specified motor speed ω and pump flow rate Q . The analysis also computed the pressure differential P across the pump inlet and outlet. The equations here are based on the model presented in [14], and much of the notation has been retained. Some modifications have been made to smooth analysis responses so that optimization can be performed more easily. Note that many of the terms used in the following equations have been defined in Tables 1 and 2.

The impeller blade tip speed at the outlet is $u_2 = \omega D_2/2$, and the radial fluid velocity relative to the impeller is $W_{m2} = Q/\pi D_2 b$. The fluid velocity leaving the impeller in the direction of the blade is $W_2 = W_{m2}/\cos(\beta_2)$. The Wiesner slip coefficient is:

$$\sigma = 1 - \frac{\sqrt{\sin(\pi/2 - \beta_2)}}{n_B^{0.7}}$$

The tangential velocity of the fluid leaving the impeller relative to a fixed coordinate system is $C_{t2} = u_2\sigma - W_{m2}\tan(\beta_2)$, and the pump theoretical head is:

$$H_{th} = u_2 C_{t2}/g$$

where g is the acceleration of gravity. The disk friction loss is

$$D_{FH} = \frac{C_{DF}\rho_c\omega^3(D_2/2)^5}{Q}$$

The fluid velocity at the inlet in the radial direction with respect to a fixed coordinate system is $C_1 = 4Q/(D_1^2 - D_s^2)\pi$. It is possible to configure a pump such that the drive shaft does not impede flow at the inlet. This is assumed to be the case, and therefore $D_s = 0$. The impeller blade tip speed at the inlet is $u_1 = \omega D_1/2$, and the velocity of the fluid entering the impeller in the direction of the blade is $W_1 = \sqrt{C_1^2 + u_1^2}$. The inlet flow angle is $\beta_{F1} = \tan^{-1}(u_1/C_1)$. Several intermediate values must be determined to calculate the skin friction head loss:

$$\beta_{s1} = 2\beta_{F1} - \beta_1$$

$$T_1 = \frac{\sqrt{\cos^2(\beta_{F1}) - \cos(\beta_1)\cos(\beta_{s1})}}{\cos(\beta_{s1})}$$

$$T_2 = \begin{cases} T_1 & \text{if } R_{t1} \geq 0 \\ -T_1 & \text{if } R_{t1} < 0 \end{cases}$$

$$R_{t1} = \cos(\beta_{F1})/\cos(\beta_{s1})$$

$$x_{L1} = R_{t1} - T_2$$

$$D_{\text{QIN12}} = \frac{W_1^2}{2gx_{L1}^2} \left(1 - \frac{x_{L1} \cos(\beta_{F1})}{\cos(\beta_1)} \right)^2$$

$$D_{\text{H12}} = \frac{bD_2\pi \cos(\beta_2)}{n_B(b + \pi D_2 \cos(\beta_2)/n_B)}$$

The skin friction head loss is:

$$D_{\text{QSF12}} = \frac{C_{\text{SF}}(D_2 - D_1)(W_2 + W_1)^2}{8g \cos(\beta_2)D_{\text{H12}}}$$

The impeller diffusion loss as presented in [14] is computed differently depending on the ratio W_1/W_2 . This introduces a discontinuity that can hinder optimization efforts. After adding an exponential transition function this loss term is:

$$D_{\text{Qdif}} = \frac{W_1^2}{8g(1 + e^{4(1.4 - W_1/W_2)})}$$

The fluid velocity approaching the pump volute is:

$$C_3 = \sqrt{\left(\frac{C_{t2}d_2}{d_3} \right)^2 + \left(\frac{Q}{\pi d_3 b_3} \right)^2}$$

The curved diffuser leading to the pump outlet as shown in Fig. 5 is the pump volute. The volute throat velocity is:

$$C_{Q3} = \frac{Q}{\pi d_3 b_3 \cos(\beta_3)}$$

The volute head loss is:

$$D_{\text{QIN23}} = \begin{cases} D_{23} & \text{if } D_{23} \geq 0 \\ 0 & \text{if } D_{23} < 0 \end{cases}$$

where $D_{23} = C_{\text{in}}(C_3^2 - C_{Q3}^2)/2g$. The diffuser skin friction loss is:

$$D_{\text{QSF34}} = C_{\text{SF}} \frac{(d_3 - d_1)(C_{Q3} + C_1)^2}{8g \cos(\beta_3) \frac{b_3 d_3 \pi \cos(\beta_3)}{b_3 n_V + d_3 \pi \cos(\beta_3)}}$$

The diffuser expansion loss term in [14] is calculated differently depending on the value of C_{Q3}/C_1 . Another transition curve is defined here to eliminate the discontinuity:

$$\varphi_{\text{QVD}} = \frac{1}{1 + e^{4(1.4 - C_{Q3}/C_1)}}$$

The diffuser expansion loss is:

$$D_{\text{QVD}} = \begin{cases} D_{24} & \text{if } D_{24} \geq 0 \\ 0 & \text{if } D_{24} < 0 \end{cases}$$

where:

$$D_{24} = \frac{(C_{\text{VD}} + \varphi_{\text{QVD}}/4)C_{Q3}^2 - C_1^2 \phi_{\text{QVD}}/2}{2g}$$

The actual head developed by the pump is:

$$H_{ac} = H_{th} - D_{\text{QIN12}} - D_{\text{QSF12}} - D_{\text{QIN23}} - D_{\text{Qdif}} - D_{\text{QSF34}} - D_{\text{QVD}}$$

The pressure differential and the shaft torque can now be computed:

$$P = H_{ac} \rho c g \quad (20)$$

$$\tau = \frac{\rho g Q}{\omega} (H_{th} + D_{\text{FH}}) \quad (21)$$

7 Optimization Results

The solution to Problem (1) obtained using the mesh adaptive direct search algorithm and the IDF formulation is presented in Table 3. Numerous starting points and algorithm parameters were tested, and the solution presented is the best obtained to date. It is unknown whether this is the global solution. The stochastic nature of the optimization algorithm makes exact replication difficult, but similar results have been obtained from multiple starting points. Gradient-based algorithms have thus far failed to find a feasible solution. This optimization model has been used as an example in [7].

Table 3: Optimization results for the electric water pump design problem

| | |
|--------------------|-------------|
| $x_1 = d$ | 8.4 (mm) |
| $x_2 = d_2$ | 76.6 (mm) |
| $x_3 = d_3$ | 146 (mm) |
| $x_4 = L$ | 145 (mm) |
| $x_5 = \ell_c$ | 55.4 (mm) |
| $x_6 = D_2$ | 58.8 (mm) |
| $x_7 = b$ | 28.5 (mm) |
| $x_8 = \beta_1$ | 0.793 (rad) |
| $x_9 = \beta_2$ | 1.22 (rad) |
| $x_{10} = \beta_3$ | 0.913 (rad) |

Acknowledgments

This work was supported by a US NSF Graduate Research Fellowship, which is gratefully acknowledged. The preliminary work of Marc Zawislak in electric pump design was an instrumental foundation for developing this revised optimization model.

References

- [1] J.T. Allison, M. Kokkolaras, M. Zawislak, and P.Y. Papalambros. On the use of analytical target cascading and collaborative optimization for complex system design. In *6th World Conference on Structural and Multidisciplinary Optimization*, May 30–June 3, 2005.
- [2] J.T. Allison, M. Kokkolaras, and P.Y. Papalambros. On selection of single-level formulations for complex system design optimization. *Journal of Mechanical Design, Transactions of the ASME*, 129(9):898–906, 2007.
- [3] P.J. McCleer. Electric drives for pump, fan, and compressor loads in automotive applications. In *the Proceedings of the IEEE International Symposium on Industrial Electronics*, pages 80–85, Jul. 10-14 1995.
- [4] J. G. Kassakian. Future of power electronics in advanced automotive electrical systems. In *IEEE Annual Power Electronics Specialists Conference*, pages 7–14, 1996.
- [5] M. Kokkolaras, Z. Mourelatos, L. Louca, Z. Filipi, G. Delagrammatikas, A. Stefanopoulou, P. Y. Papalambros, and D. Assanis. Design under uncertainty and assessment of performance reliability of a dual-use medium truck with hydraulic-hybrid powertrain and fuel cell auxiliary power unit. *SAE 2005 Transactions: Journal of Passenger Cars - Mechanical Systems*, 2006. (Selected from the Proceedings of the SAE World Congress, April 11-14, 2005, Detroit, Michigan, paper no. 2005-01-1396).
- [6] B. Surampudi, J. Redfield, G. Ray, A. Montemayor, M. Walls, H. McKee, T. Edwards, and M. Lasecki. Electrification and integration of accessories on a class-8 tractor. In *the Proceedings of the SAE World Congress, SAE-2005-01-0016*, April 11-14 2005.
- [7] J.T. Allison, M. Kokkolaras, and P.Y. Papalambros. Optimal partitioning and coordination decisions in decomposition-based design optimization. In *In the Proceedings of ASME 2007 Design Engineering Technical Conferences and Computers and Information in Engineering Conference, DETC2007-34698*, Baltimore, MD, September 4-7, 2007.
- [8] M.A. Abramson, C. Audet, and J.E. Dennis Jr. Nonlinear programming with mesh adaptive direct searches. *SIAG/Optimization Views-and-News*, 17(1):2–11, 2006.
- [9] E. J. Cramer, J. E. Dennis, P. D. Frank, R. M. Lewis, and G. R. Shubin. Problem formulation for multidisciplinary optimization. *SIAM Journal of Optimization*, 4:754–776, 1994.
- [10] P.H. Mellor, D. Roberts, and D.R. Turner. Lumped parameter thermal model for electrical machines of TEFC design. *IEE Proceedings B: Electric Power Applications*, 138(5):205–218, 1991.
- [11] F.P. Incropera and D.P. DeWitt. *Introduction to Heat Transfer*. John Wiley and Sons, Inc., 2002.
- [12] T. Kenjo and S. Nagamori. *Permanent-Magnet and Brushless DC Motors*. Oxford University Press, New York, 1985.
- [13] J. F. Gieras and M. Wing. *Permanent Magnet Motor Technology*. Marcel Dekker, Inc., New York, 2002.
- [14] J. Tuzson. *Centrifugal Pump Design*. John Wiley and Sons, New York, 2000.